MoW synergetic effect supported by HAADF for alumina based catalysts prepared from mixed SiMo$_n$W$_{12-n}$ heteropolyacids

Maria Nikulshina[a,b], Alexander Mozhaev[a], Christine Lancelot[b], Maya Marinova[c], Pascal Blanchard[b], Edmond Payen[b], Carole Lamonier[b,**], Pavel Nikulshin[a,d,*]

[a] Samara State Technical University, 244 Molodogvardeiskaya st., Samara 443100, Russia
[b] Univ. Lille, CNRS, Centrale Lille, ENSCL, Univ. Artois, UMR 8181 – UCCS – Unité de Catalyse et Chimie du Solide, F-59000 Lille, France
[c] Institut Chevreul, University of Lille & CNRS, Villeneuve dAscq F-59655, France
[d] All-Russian Research Institute of Oil Refining, 6/1 Aviamotornaya st., Moscow 111116, Russia

ARTICLE INFO

ABSTRACT

MoW catalysts supported on Al$_2$O$_3$ with equal surface content of metals (Mo + W = 3.9 at/nm^2) were synthesized by using mixed Keggin type heteropolyacids (HPAs) H$_4$[SiMo$_1$W$_{11}$O$_{40}$] and H$_4$[SiMo$_3$W$_9$O$_{40}$] and corresponding mixture of monometallic H$_4$[SiMo$_{12}$O$_{40}$] and H$_4$[SiW$_{12}$O$_{40}$] HPAs. After liquid phase sulfidation, catalysts were characterized by high-resolution transmission electron microscopy (HRTEM) and X-ray photoelectron spectroscopy (XPS). For the first time, High Angle Annular Dark Field microscopy (HAADF) was used to evidence the morphology and composition of the active sulfide phase. The catalysts were tested in hydrotreating of model feed that contained dibenzothiophene (DBT) and naphthalene. Using mixed SiMo$_n$W$_{12-n}$HPAs as starting precursors had a beneficial effect on the catalytic activity. Incorporation of molybdenum in the structure of SiW Keggin-type HPA led to a decrease of the size of active phase crystallites, to an increase of the metal sulfidation degree and of the number of active sites. Substitution of a quarter of tungsten atoms by molybdenum allowed to achieve DBT conversion comparable to value obtained on pure SiMo$_{12}$HPA based catalyst and higher conversion of naphthalene. Both SiMo$_n$W$_{12-n}$HPAs based catalysts had higher rate constants in studied reactions compared to their corresponding references prepared from two separate monometallic HPAs. Moreover, Mo$_n$W$_{12-n}$/Al$_2$O$_3$ catalysts had the highest selectivity in respect of hydrogenation (HYD) pathway of DBT hydrodesulfurization (HDS). The presence of mixed Mo$_x$W$_{1-x}$S$_2$ slabs was evidenced by HAADF analysis. On Mo$_3$W$_9$/Al$_2$O$_3$, small randomly distributed islands of Mo were present in the WS$_2$ slabs, while on Mo$_3$ + W$_9$/Al$_2$O$_3$, Mo islands appeared larger and in the core of the WS$_2$ slabs. Moreover, on this last sample, some monometallic slabs were also present. It was concluded that using mixed HPA precursors resulted in the formation of mixed Mo$_x$W$_{1-x}$S$_2$ active phase possessing higher synergetic effect between the two metals and consequently higher catalytic activity.

1. Introduction

The main complication in the oil refining industry is associated to more stringent environmental requirements for motor fuels (transport fuels) namely, set to reduce the content of sufur-containing compounds. One of the key approaches to meet these standards is the development of new highly active HDS catalysts that allow producing ultra-low sulfur fuels. Typically, Co(Ni)Mo(W) catalysts supported on alumina are used in the hydrotreating reactions. The development of the trimetallic NiMoWS bulk catalyst «Nebula» in the early 2000 allowed to reach a new level of activity for hydrotreating catalysts. This catalyst exhibits activity at least three times higher than any other hydrotreating catalyst conventionally used in industry [1]. P. Raybaud and co-workers [2] predicted a synergetic effect for Ni promoted Mo$_{1-x}$W$_x$S$_2$ active phases. It was reported that NiMoWS$_2$ phases should be more active than NiMoS and NiWS ones. For CoMo$_{1-x}$W$_x$S$_2$ phases, weak synergetic effect was observed with respect to CoMoS and CoWS ones. Olivas et al. [3] confirmed that the synergetic effect of Ni is higher in mixed (Mo-W)S$_2$ clusters than in supported Ni(MoS$_2$) and Ni(WS$_2$) separated catalysts. Therefore, trimetallic Ni–Mo–W sulfide catalysts have a potential advantage over bimetallic Ni-Mo and Ni-W systems, in respect to deep sulfur and nitrogen removal. However, the precise determination of the

* Corresponding author at: Samara State Technical University, 244 Molodogvardeiskaya st., 443100, Samara 443100, Russia.
** Corresponding author.
E-mail addresses: carole.lamonier@univ-lille1.fr (C. Lamonier), p.a.nikulshin@gmail.com (P. Nikulshin).

reasons of the high activity of these catalysts is not simple. Some authors supposed that mixed Ni-Mo-W active sites are formed [4]. However, the experimental investigations of bimetallic mixed Mo-W active sites are scarce. At the same time, the development of effective ways to form mixed Mo-WS$_2$ slabs seems to be a key to design new highly effective hydroprocessing catalysts. In this work, we report the preparation of alumina supported MoW catalysts using mixed bimetallic Si-Mo$_n$W$_{12-n}$ Keggin type heteropolyacids (HPAs). Their performance in the hydrotreating reactions of DBT and naphthalene was evaluated and compared to that of reference catalysts obtained from a mixture of two monometallic Mo and W based HPAs. Besides classical characterizations of sulfide catalysts (HRTEM and XPS), an innovative HAADF characterization allowing to distinguish between Mo and W atoms in the disulfide slabs active phase is presented for the first time.

2. Experimental

2.1. Catalyst preparation

Two heteropolyacids of H$_4$[SiMo$_1$W$_{11}$O$_{40}$] (hereafter SiMo$_1$W$_{11}$) and H$_4$[SiMo$_3$W$_9$O$_{40}$] (hereafter SiMo$_3$W$_9$) were synthesized according to previous report [5], where their elemental composition and structures were confirmed by XRD, IR-, Raman spectroscopy and EXAFS. Catalysts with surface density of metals d(Mo + W) equal to 3.9 at.nm^{-2} were prepared by incipient wetness technique via impregnation of γ-Al$_2$O$_3$ extrudates (S$_{BET}$ = 230 m^2/g, V$_p$ = 0.9 cm^3/g) with aqueous solutions containing the required amounts of SiW$_{11}$Mo$_1$ and SiW$_9$Mo$_3$. These solids will be referred to as Mo$_1$W$_{11}$/Al$_2$O$_3$ and Mo$_3$W$_9$/Al$_2$O$_3$. The catalysts based on monometallic SiMo$_{12}$ and SiW$_{12}$ were prepared for comparison and denoted Mo$_{12}$/Al$_2$O$_3$ and W$_{12}$/Al$_2$O$_3$, respectively. Two bimetallic samples with a Mo/W ratio of 1/11 and 3/9 corresponding to the composition of the mixed SiMo$_n$W$_{12-n}$ were synthesized using a mixture of monometallic Mo and W HPAs and will be denoted Mo$_1$ + W$_{11}$/Al$_2$O$_3$ and Mo$_3$ + W$_9$/Al$_2$O$_3$. After impregnation and maturation, the catalysts were dried at 100 °C for 10 h in air atmosphere without calcination. The chemical compositions of the prepared catalysts are given in Table 1.

For characterization of the active phase, the samples were sulfided following the procedure used for activation prior to the catalytic test: a mixture of dimethyldisulfide (DMDS, 2 wt.% of sulfur) and decane at 3.5 MPa was utilised in a stepwise protocol conducted over 10 h at 240 °C and 8 h at 340 °C.

2.2. Characterization of the catalysts

2.2.1. Textural characteristics of the oxidic precursors

The textural characteristics of the prepared oxide precursors were determined by nitrogen adsorption performed at 77 K on a Quantachrome Autosorb-1 adsorption porosimeter. The specific surface area (SSA) was calculated using the Brunauer-Emmett-Teller method at relative partial pressures (P/P$_0$) ranging from 0.05 to 0.3. The total pore volumes (at P/P$_0$ of 0.99) and pore size distributions were calculated based on the desorption curve using the Barret-Joyner-Halenda model. Before the measurement, the samples were outgassed under vacuum (< 10^{-1}Pa) at 350 °C for 4 h.

2.2.2. Temperature-programmed reduction (TPR)

TPR analyses of the synthesized catalysts were carried out on a TPDRO 1100 Series multifunction adsorption instrument and were conducted with a mixture of 5 vol.% H$_2$ in N$_2$. The TPR profiles were recorded with the use of a thermal conductivity detector (TCD) under a volume flow rate of 25 ml/min, a temperature range from room temperature to 1000 °C, a heating rate of 10°/min and a holding period of 1 h at 1000 °C.

2.2.3. High-resolution transmission electron microscopy (HRTEM)

HRTEM was carried out using a Tecnai G2 20 electron microscope with a 0.14 nm lattice-fringe resolution and an accelerating voltage of 200 kV. Freshly sulfided samples were ground under an inert atmosphere and dispersed in ethanol. The suspension was collected on carbon films supported on copper grids and 10–15 representative micrographs were obtained for each catalyst in high–resolution mode. Typically, the length and stacking of at least 500 slabs were measured for each catalyst. Distributions in length and stacking of the slabs were determined. To measure the extent of Mo(W)S$_2$ dispersion, the average fraction of Mo(W) atoms at the Mo(W)S$_2$ edge surface (D) was calculated, assuming that the Mo(W)S$_2$ slabs were perfect hexagons [6]. Mo(W)S$_2$ dispersion (D) was statistically evaluated by dividing the total number of Mo(W) atoms at the edge surface (W$_e$), including corner sites (W$_c$), by the total number of Mo(W) atoms (W$_T$) using the slab sizes measured in the TEM micrographs:

$$D = \frac{W_e + W_c}{W_T} = \frac{\sum_{i=1..t} 6n_i - 6}{\sum_{i=1..t} 3n_i^2 - 3n_i + 1},$$

(1)

where n_i is the number of Mo(W) atoms along one side of the Mo(W)S$_2$ slab, as determined by its length, and t is the total number of slabs in the TEM micrograph.

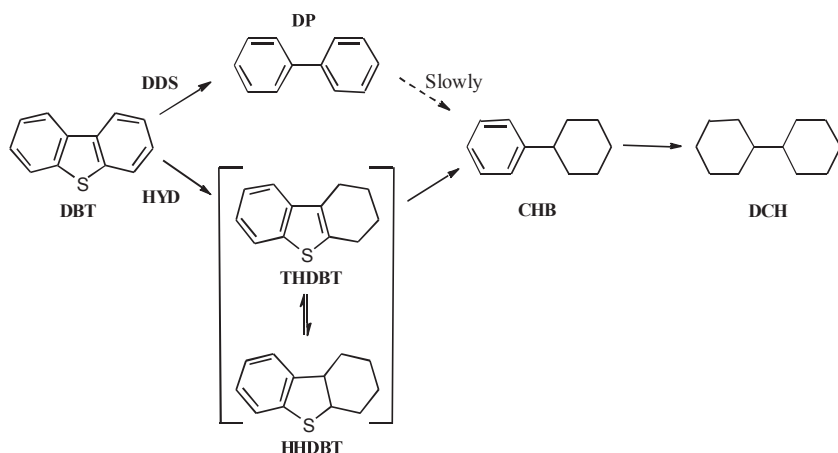The number of slabs per stack was determined to obtain the average stacking degree ($\overline{N}$):

$$\overline{N} = \frac{\sum_{i=1..t} n_i N_i}{\sum_{i=1..t} n},$$

(2)

where n_i is the number of stacks in N_i layers.

High resolution high-angle annular dark-field (HRHAADF) imaging has been performed at 200 kV on a TITAN Themis FEI scanning transmission electron microscope (S/TEM). The microscope is equipped with a monochromator and a Cs probe corrector. For HAADF acquisition, the spot size was 9 with a screen current of ~50 pA and a camera length of 115 mm, corresponding to inner and outer diameters of the annular detector of ~50 and ~200 mrad, respectively. The samples were prepared in the same way as for HRTEM analysis. More than 50 slabs were observed on each studied catalyst.

2.2.4. X-ray photoelectron spectroscopy (XPS)

The sulfided catalysts were analysed by XPS. The spectra were obtained on a Kratos Axis Ultra DLD spectrometer using a monochromatic AlK$_a$ source (hn = 1486.6 eV, 150 W). The binding energy (BE) scale of the spectrometer was preliminarily calibrated using the position of the peaks for the Au 4f$_{7/2}$ (83.96 eV) and Cu 2p$_{3/2}$ (932.62 eV) core levels of pure metallic gold and copper. The samples were mounted on a holder using double-sided adhesive tape. For the non-conductive samples, the Kratos charge neutraliser system was used and the spectra were charge-corrected to provide the C 1s spectral component of

Table 1
Composition and textural properties of prepared Mo$_n$W$_{12-n}$/Al$_2$O$_3$ catalysts.

Catalyst	MoO$_3$ (wt%)	WO$_3$ (wt%)	Specific surface area (m^2/g)	Pore volume (cm^3/g)	Average pore diameter (Å)
Mo$_{12}$/Al$_2$O$_3$	18.0	–	215	0.53	7.6
W$_{12}$/Al$_2$O$_3$	–	26.2	208	0.54	7.6
Mo$_1$W$_{11}$/Al$_2$O$_3$	1.4	24.2	205	0.52	7.5
Mo$_3$W$_9$/Al$_2$O$_3$	4.2	20.1	210	0.54	7.6
Mo$_1$ + W$_{11}$/ Al$_2$O$_3$	1.4	24.2	208	0.56	7.5
Mo$_3$ + W$_9$/ Al$_2$O$_3$	4.2	20.1	217	0.55	7.5

Scheme 1. Reaction network of the HDS of DBT.

adventitious carbon (C—C, C—H) at 284.8 eV. In addition to the survey photoelectron spectra, narrow spectral regions (Al 2p, S 2p, Mo 3d, W 4f, C 1s and O 1s) were recorded. The pass energy of the analyzer was 160 eV for the survey spectra and 40 eV for the narrow scans. The individual spectral regions were analyzed to determine the BE of the peaks, identify the chemical state of the elements and calculate the relative ratios of the elements on the catalyst surface.

The collected spectra were analysed using the CasaXPS software program (Version 2.3.16) after applying a Shirley background subtraction. Gaussian (30%) − Lorentzian (70%) peaks were used for spectra decomposition. The decompositions of the S 2p, Mo 3d and W 4f XPS spectra were performed using the appropriate oxide and sulfided references as supported monometallic catalysts [7–9].

XPS decomposition enabled the absolute quantification of each species:

$$C(j)_T \ (\text{at.%}) = \frac{A_j / S_j}{\sum\limits_{i=1..n} A_i / S_i} \times 100, \tag{3}$$

where A_i is the measured area of species i, S_i is the sensitivity factor of the atom related to species i (provided by the manufacturer) and $C(j)_T$ is the absolute content of species j.

The relative concentrations of each species Mo^{6+}, MoS_xO_y, MoS_2, W^{6+}, WS_xO_y and WS_2 were determined for all sulfided catalysts. For example, the relative amount of WS_2 was determined using the following equation:

$$[WS_2] \ (\%) = \frac{A_{WS_2}}{A_{WS_2} + A_{WS_xO_y} + A_{W^{6+}}} \times 100, \tag{4}$$

where A_X represents the peak area of species x.

The absence of any signal at 169.0 eV (characteristic of sulfates) indicates that the sulfided catalysts were not reoxidized during the transfer of the solids from the sulfiding reactor to the XPS instrument.

2.3. Evaluation of the catalytic activities

The DBT HDS and naphthalene HYD tests were performed in a fixed-bed microreactor under 320 °C, 3.0 MPa of hydrogen, with a LHSV (liquid hourly space velocity) of 10 h^{-1} and a 500 NL/L volume ratio of hydrogen to feed. In a typical experiment, 0.6 g of the catalyst (0.25–0.50 mm) was diluted with 0.6 cm^3 of low-surface-area carborundum (0.2–0.4 mm) and placed in the centre of the reactor (with an internal diameter of 0.8 cm). Prior to the catalytic activity tests, the oxidic precursors were sulfided with a mixture of DMDS (2 wt.% of sulfur) and decane at 3.5 MPa in a stepwise procedure over 10 h at 240 °C and 8 h at 340 °C. A mixture of DBT (1000 ppm S), naphthalene (3 wt.%), hexadecane (as an internal standard, 1 wt.%) and toluene (as

a solvent) was used as a model feedstock for evaluation of HDS and HYD performances. The liquid product compositions of the samples collected every hour were determined using a Crystall-5000 Gas Chromatograph equipped with a 30 m OV-101 column. The reaction products were identified by matching retention times with those of commercially available standards and by GC/MS analysis using a Finnigan Trace DSQ. All catalysts exhibited stable performance, achieving a steady state after 7–10 h.

The rate constants of the pseudo-first-order reactions of the DBT HDS and naphthalene HYD were determined using the following equations:

$$k_{HDS} = -\frac{F_{DBT}}{W} \ln(1 - x_{DBT}) \quad \text{and} \quad k_{HYD} = -\frac{F_{Naph}}{W} \ln(1 - x_{Naph}), \tag{5}$$

where k_{HDS} and k_{HYD} are the pseudo-first-order reaction constants for the DBT HDS and naphthalene HYD (mol g^{-1} h^{-1}) respectively, x_{DBT} and x_{Naph} are the conversions (%) of DBT and naphthalene respectively, F_{DBT} and F_{Naph} are the reactant flow in moles (mol h^{-1}) and W is the catalyst mass (g).

The products of the HDS of DBT included biphenyl (BP) via the direct desulfurization (DDS) pathway, as well as cyclohexylbenzene (CHB) and dicyclohexyl (DCH) from the HYD pathway. Only traces of hydrogenated tetrahydro- and hexahydrodibenzothiophenes were observed. The HYD/DDS selectivity was calculated according to the reaction network for DBT HDS (Scheme 1):

$$S_{HYD/DDS} = \frac{k_{HYD}}{k_{DDS}} = \frac{C_{CHB} + C_{DCH}}{C_{BP}}, \tag{6}$$

where C_{CHB}, C_{BCH} and C_{BP} are the concentrations (wt.%) of CHB, DCH and BP in the reaction products respectively.

The turnover frequencies (TOF, s^{-1}) normalised on edge sites of Mo(W)S$_2$ slabs for the HDS of DBT and HYD of naphthalene allowed to get a more complete understanding of the catalytic properties of the active phase species. TOF values were calculated using the following equations:

$$TOF_{HDS} = \frac{F_{DBT} \cdot x_{DBT}}{W \cdot \left(\frac{C_{WS_2}}{Mr_W} + \frac{C_{MoS_2}}{Mr_{Mo}}\right) \cdot D \cdot 3600} \quad \text{and} \quad TOF_{HYD} = \frac{F_{Naph} \cdot x_{Naph}}{W \cdot \left(\frac{C_{WS_2}}{Mr_W} + \frac{C_{MoS_2}}{Mr_{Mo}}\right) \cdot D \cdot 3600}, \tag{7}$$

where F_{DBT} and F_{Naph} are the reactant flow (mol h^{-1}), x_{DBT} and x_{Naph} are the conversions (%) of DBT and naphthalene, W is the catalyst mass (g), C_{WS_2} and C_{MoS_2} are the effective content of W and Mo in Mo(W)S$_2$ species (wt.%), D is the dispersion of Mo(W)S$_2$ species; Mr_W and Mr_{Mo} are the molar mass of tungsten (183.9 g/mol) and molybdenum (95.9 g/mol).
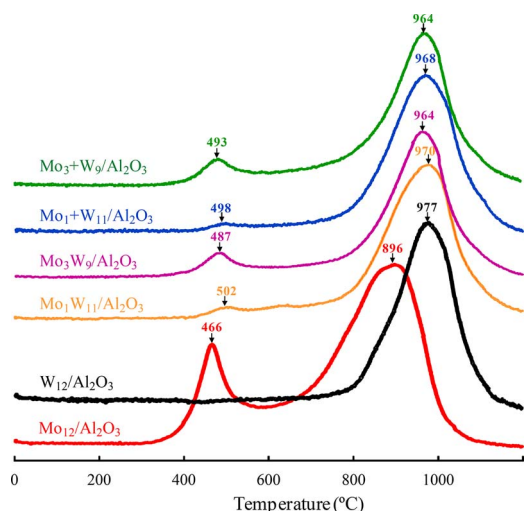
Fig. 1. H$_2$-TPR profiles for oxidic Mo$_n$W$_{12-n}$/Al$_2$O$_3$ catalysts.

3. Results

3.1. Characterization of the oxidic precursors

The amount of loaded metals and the textural characteristics of synthesized oxidic precursors are shown in Table 1. No significant decrease in surface area and pore volume was observed when metals were deposited on the support, indicating the absence of large metallic based particles.

Reduction profiles of oxidic Mo$_n$W$_{12-n}$/Al$_2$O$_3$ samples are presented in Fig. 1. The reduction profile of Mo$_{12}$/Al$_2$O$_3$ sample exhibited two maxima at 466 and 896 °C. The low-temperature H$_2$ consumption peak is associated to the first reduction step (Mo^{6+} → Mo^{4+}) of octahedral molybdenum species weakly bound to the alumina support. The high-temperature peak corresponds to the second reduction step (Mo^{4+} → Mo^0) of polymeric octahedral Mo species strongly bound to the support [10,11]. The TPR profile of W$_{12}$/Al$_2$O$_3$ displays only one maximum at 977 °C, which can be associated to the reduction of dispersed W species of various reducibilities [12].

The reduction profiles of all bimetallic solids show two main peaks. The low-temperature consumption peaks in the TPR profile of MoW samples were slightly shifted towards higher temperatures compared to pure Mo$_{12}$/Al$_2$O$_3$. The intensity of the low-temperature TCD signals is correlated to the Mo contents in the samples (Table 2). It should also be mentioned that the reduction temperature of Mo$_3$W$_9$/Al$_2$O$_3$ sample was the lowest (487 and 964 °C) among the bimetallic catalysts. Mo and W in the oxidic Mo$_n$W$_{12-n}$/Al$_2$O$_3$ samples have similar H$_2$ consumption (reduction properties).

Table 2-
H$_2$ consumption of the oxide Mo$_n$W$_{12-n}$/Al$_2$O$_3$ catalysts during the H$_2$-TPR analyses.

Catalyst	T_{max} (°C)	H$_2$ (mmol/g)	T_{max} (°C)	H$_2$ (mmol/g)	Total H$_2$ (mmol/g)
Mo$_{12}$/Al$_2$O$_3$	466	310	896	1567	1877
W$_{12}$/Al$_2$O$_3$	–	–	977	1307	1307
Mo$_1$W$_{11}$/Al$_2$O$_3$	502	26	970	1372	1397
Mo$_3$W$_9$/Al$_2$O$_3$	487	100	964	1215	1315
Mo$_1$ + W$_{11}$/Al$_2$O$_3$	498	20	968	1335	1355
Mo$_3$ + W$_9$/Al$_2$O$_3$	493	90	964	1232	1322

3.2. Characterization of sulfided catalysts

3.2.1. HRTEM

Sulfided Mo$_n$W$_{12-n}$/Al$_2$O$_3$ catalysts were characterized by HRTEM in order to obtain more information about the dispersion of Mo(W)S$_2$ crystallites. The HRTEM micrographs show the typical fringes due to Mo(W)S$_2$ crystallites with 0.65 nm interplanar distances (Fig. 2). The distributions in stacking degree and slab length of the samples as well as the corresponding average values are presented in Table 3. The average stacking degree varied between 1.3 and 1.7. The catalysts synthesized with mixed SiMo$_n$W$_{12-n}$ showed slightly smaller length of Mo(W)S$_2$ particles (4.4 for Mo$_1$W$_{11}$/Al$_2$O$_3$ and 4.8 for Mo$_3$W$_9$/Al$_2$O$_3$) than that of monometallic references (4.7 for Mo$_{12}$/Al$_2$O$_3$ and 4.9 for W$_{12}$/Al$_2$O$_3$) and significantly smaller than that of bimetallic samples prepared using the mixtures of monometallic SiMo$_{12}$ and SiW$_{12}$ (5.1 for Mo$_1$ + W$_{11}$/Al$_2$O$_3$ and 5.3 for Mo$_3$ + W$_9$/Al$_2$O$_3$).

3.2.2. HAADF

Typical HAADF images of sulfided Mo$_3$W$_9$/Al$_2$O$_3$ and Mo$_3$ + W$_9$/Al$_2$O$_3$ catalysts are presented in Fig. 3 and reveal the 2D morphology of the sulfided slabs. Indeed this technique allows to visualize the basal planes of the sulfide phase which cannot be observed by TEM. Compared to solids supported on model carriers, more irregular shapes are observed [13,14] which can be related to the interaction of the active phase with the irregular surface of the alumina. Small clusters (< 1 nm) and isolated atoms are also evidenced, which presence is not visible by TEM (Fig. 2).

On sulfided mixed Mo$_3$W$_9$/Al$_2$O$_3$ and Mo$_3$ + W$_9$/Al$_2$O$_3$ catalysts, differences in contrast between atoms in the slabs are clearly observed (Fig. 3). Since the annular dark field images are formed by collecting electrons scattered at high angles, the intensities of the atomic columns in the HAADF images increase with the atomic number Z of the atom as approximately Z$^{1.7}$ [15]. This technique can thus be used to study metal atom distribution within monolayer catalysts. The intensity difference observed in the MoW solids is due to the difference in Z between Mo and W, where brighter atoms are W (Z = 74) and slightly darker atoms are Mo (Z = 42). A special attention has been taken to observe non-overlapping catalysts (i.e. monolayers) on a flat surface of the alumina support The ratio of the intensities estimated from profiles taken from a row of atoms in the slabs correspond to the difference in atomic number of tungsten and molybdenum.

This observation clearly evidences the formation of mixed slabs, with W (bright atoms) and Mo (dark atoms) in the same sulfided entity. Moreover, Mo atoms appear to be more in the core of the slabs. In Mo$_3$W$_9$/Al$_2$O$_3$, isolated Mo islands are randomly distributed inside the tungsten slabs. In the case of Mo$_3$ + W$_9$/Al$_2$O$_3$, Mo atoms appear to be gathered in larger islands in the middle of W atoms and monometallic slabs are also observed. Haandel et al. [4] also evidenced mixed structures for Ni-Mo-W catalysts prepared from conventional precursors and sulfided under gas and liquid phase sulfidation. They proposed through EXAFS analysis the formation of core-shell structures with Mo in the core and W in the outer rim of the MS$_2$ particles under gas phase activation, while more homogeneous distribution of the Mo atoms in the slabs was predicted under liquid phase sulfidation.

3.2.3. XPS spectroscopy

More detailed information about the nature of the species formed after catalyst sulfidation were obtained by XPS analysis. Fig. 4 shows examples of the decomposition of Mo 3d, W 4f and S 2p photoelectron spectra recorded for the Mo$_n$W$_{12-n}$/Al$_2$O$_3$ catalysts. The W 4f spectra contain three W 4f doublets: the doublet with binding energies at 32.1 and 34.3 eV is associated to W^{4+} species of the WS$_2$ phase, the doublet with binding energies at 33.0 and 35.2 eV to W^{5+} species of a WS$_x$O$_y$ oxysulfide species, and finally the doublet with binding energies at 36.0 and 37.9 eV to W^{6+} oxide species. On the Mo3d spectra, the signals at 229.0 eV and 232.0 eV correspond to the MoS$_2$ species. The doublet
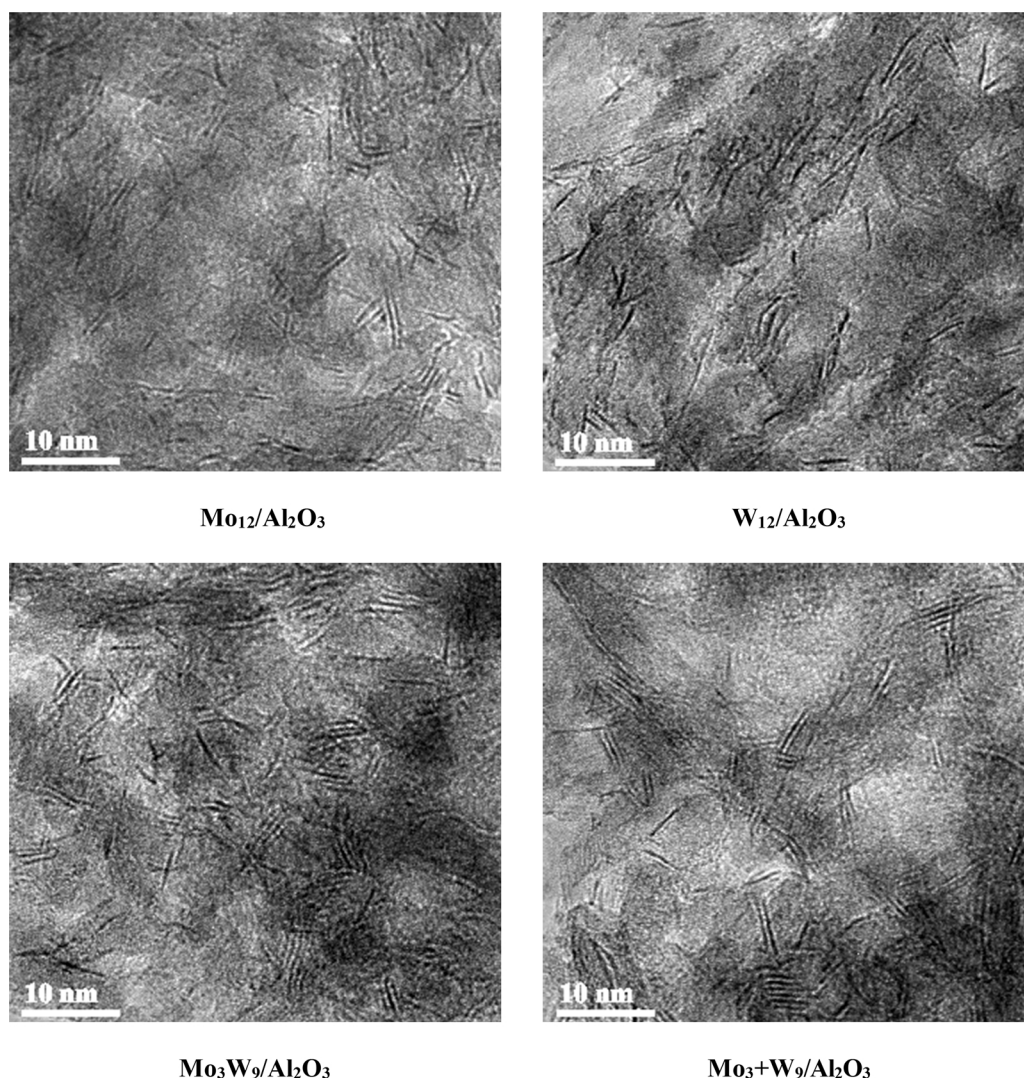
Fig. 2. HRTEM micrographs of sulfided Mo_nW_{12-n}/Al_2O_3 catalysts.

Table 3
Morphological characteristics of the $Mo(W)S_2$ active phase species calculated from TEM micrographs.

Catalyst	Average length $\overline{L}$ (nm)	Average stacking number $\overline{N}$	Dispersion of $Mo(W)S_2$ D^a	Distribution of slab length (rel.%)					Distribution of stacking number (rel.%)			
				< 2	2.4	4.6	6.8	> 8	1	2	3	> 3
Mo_{12}/Al_2O_3	4.7	1.6	0.25	4	36	39	14	7	55	33	10	2
W_{12}/Al_2O_3	4.9	1.3	0.24	4	36	36	13	11	77	19	4	–
Mo_1W_{11}/Al_2O_3	4.4	1.3	0.27	8	41	34	11	6	72	24	4	–
Mo_3W_9/Al_2O_3	4.8	1.7	0.25	3	35	40	13	9	52	30	13	5
$Mo_1 + W_{11}/Al_2O_3$	5.1	1.7	0.24	4	31	39	15	11	69	24	6	1
$Mo_3 + W_9/Al_2O_3$	5.3	1.7	0.23	1	32	39	18	10	50	38	9	3

[a] $Mo(W)S_2$ dispersion calculated from HRTEM results (Eq. (1)).

with binding energies at 230.0 and 233.5 eV is related to oxysulfide species. The doublet with binding energies at 232.5 and 235.7 eV is correlated to Mo^{6+} oxide species. The decomposition of S2 s photopeaks presented two contributions assigned to sulfide (226.0 eV) and oxysulfide entities (227.5 eV).

The results of the XPS spectra decomposition revealed the metal fractions of molybdenum and tungsten species present on the surface of the sulfided Mo_nW_{12-n}/Al_2O_3 catalysts, summarized in Table 4. The sulfidation degree of tungsten in W_{12}/Al_2O_3 was found significantly lower than that of molybdenum in Mo_{12}/Al_2O_3 (56% against 73%), which is in agreement with literature data [8,4]. In all bimetallic catalysts, the sulfidation degree of molybdenum remained identical

(100%) while the sulfidation degree of tungsten was found higher than in monometallic sample, with values between 70 and 80%. It is known that the formation of the active sulfide phase from tungsten oxide occurs at higher temperature compared to molybdenum oxide due to thermodynamics and lower reactivity [16]. It can thus be suggested that sulfidation in Mo and W based catalysts begins with the formation of MoS_2 nuclei, which contributed to activation of H_2S and thus allowed increasing sulfidation degree of WO_3 and raising the number of active sites, that is in good agreement with the HAADF results. Moreover, it should be noted that using the mixed $SiMo_3W_9$ as starting precursor led to the highest sulfidation degree of tungsten, with an increase of 10% compared to the $Mo_3 + W_9/Al_2O_3$ sample, indicating that the
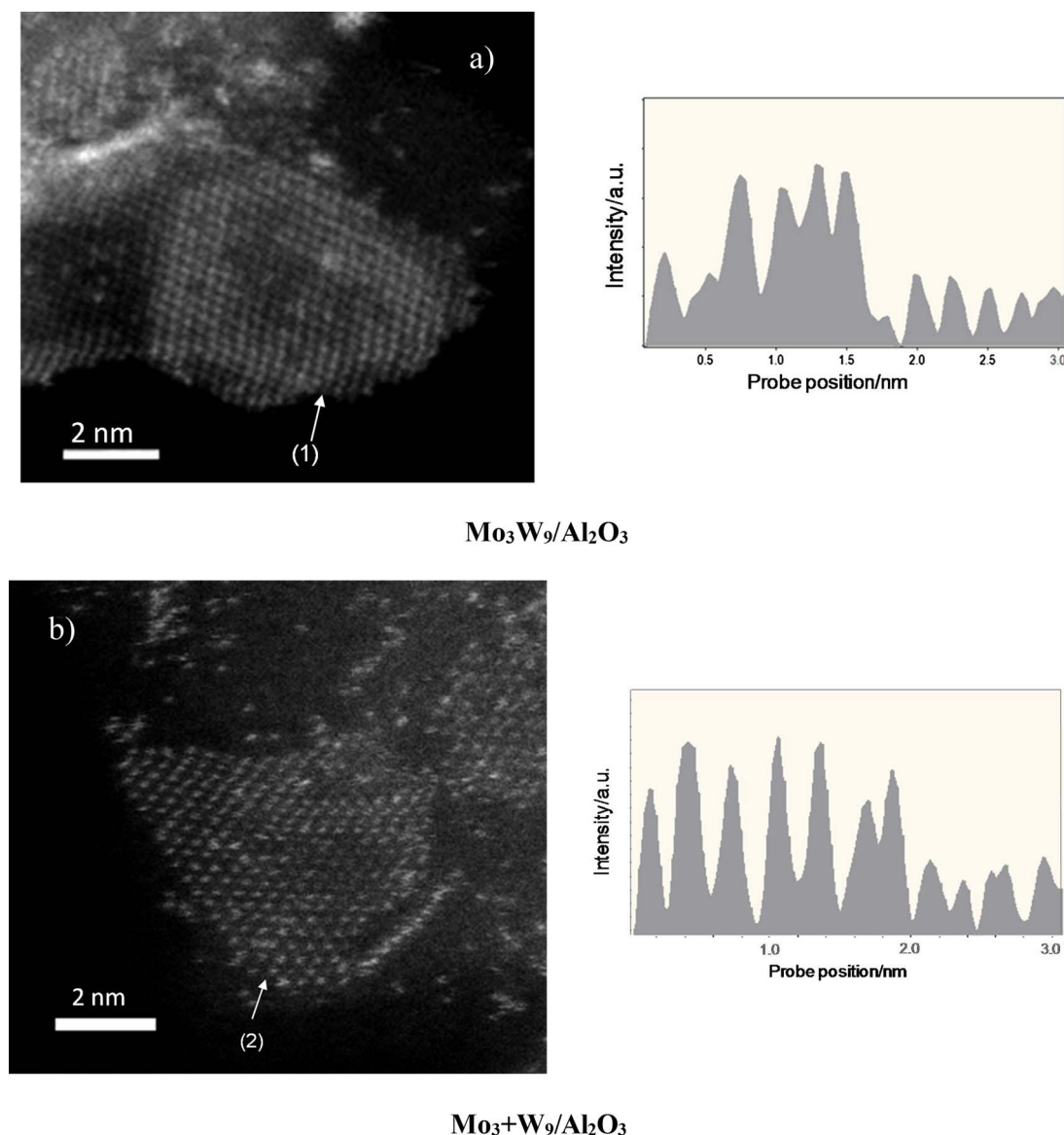
Mo₃W₉/Al₂O₃

Mo₃+W₉/Al₂O₃

Fig. 3. HAADF images of sulfided Mo₃W₉/Al₂O₃ (a) and Mo₃ + W₉/Al₂O₃ (b) catalysts with intensity profiles corresponding to the row of atoms identified by the arrows ((1) on Mo₃W₉/Al₂O₃ and (2) on Mo₃ + W₉/Al₂O₃).

proximity of Mo and W in the HPA entity all the more favors tungsten sulfidation. Full sulfidation degree of molybdenum in bimetallic catalysts (100%) could be attributed to the smaller molybdenum amount (1.4 and 4.2 wt% of MoO_3) than in monometallic sample Mo_{12}/Al_2O_3 (18 wt% of MoO_3). Also, all Mo_nW_{12-n}/Al_2O_3 catalysts contained large amount of oxidic W species that prevent strong interaction of oxidic Mo-related species with the alumina surface.

3.3. Catalytic activities

The catalytic activities of the sulfided Mo_nW_{12-n}/Al_2O_3 catalysts in HDS of DBT and hydrogenation of naphthalene are presented in Table 5. The reactants conversions varied in a wide range, from 2.9 to 30.5% for DBT HDS and from 3.9 to 31.4% for naphthalene HYD over all prepared catalysts. The W_{12}/Al_2O_3 catalyst demonstrated the lowest activities in DBT HDS as well as in naphthalene HYD. On the contrary, monometallic Mo_{12}/Al_2O_3 sample achieved the highest conversion value in DBT HDS and a high value in naphthalene HYD. This result is usually attributed to higher sulfidation degree of molybdenum compared to that of tungsten. Indeed a stronger W-O bond delays the formation of WS_2 phase compared to that of MoS_2 phase at a given

sulfidation temperature [17,18]. Both catalysts $Mo_1 + W_{11}/Al_2O_3$ and $Mo_3 + W_9/Al_2O_3$ prepared from two monometallic HPA demonstrated a much lower activity than the monometallic Mo_{12}/Al_2O_3 sample both in HDS and HYD. The measured conversions were however much higher than those of the monometallic W_{12}/Al_2O_3, multiplied by more than 3 with the presence of 1 atom of Mo for 11 atoms of W and by 4 for $Mo_3 + W_9/Al_2O_3$ for DBT HDS, and between 2 and 2.4 times for the HYD of naphthalene. Moreover, the catalysts synthesised via mixed $SiMo_nW_{12-n}$ had higher HDS and HYD performances than their MoW/Al_2O_3 analogues with the same metal contents. The conversion of Mo_3W_9/Al_2O_3 is similar to that of Mo_{12}/Al_2O_3 catalyst in the HDS of DBT (around 30%) and is much higher than that of Mo_{12}/Al_2O_3 in the HYD of naphthalene (31.4 versus 24.0%). The presence of decaline in reaction products has not been detected over all catalysts due to chosen conditions of catalytic experiments that allowed us to measure the catalytic properties at low reactant conversions.

4. Discussion

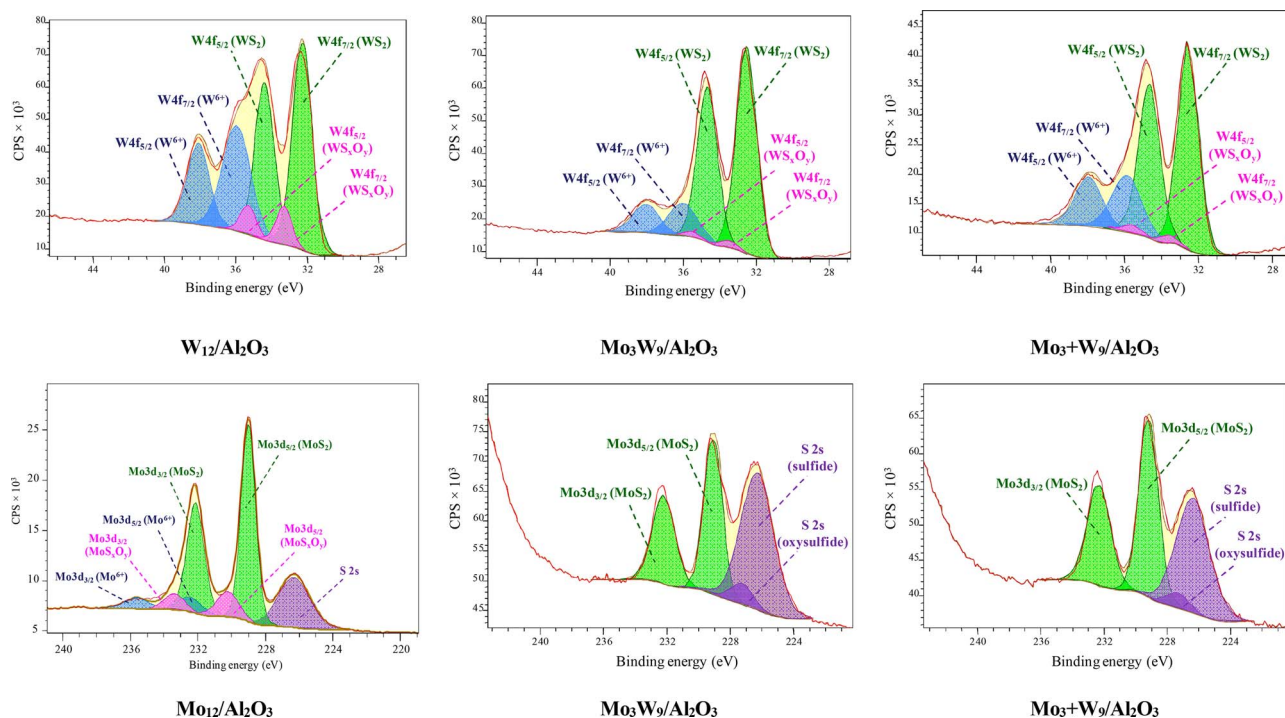The presence of a small quantity of molybdenum in the Mo + W/Al_2O_3 catalysts prepared from a mixture of $SiMo_{12}$ and SiW_{12} has a

Fig. 4. XPS W 4f and Mo 3d spectra recorded for Mo_nW_{12-n}/Al_2O_3 catalysts; in blue: $Mo(W)^{6+}$ oxide contributions; in pink: $Mo(W)S_xO_y$ contributions; in green: $Mo(W)S_2$ contributions (For interpretation of the references to color in this figure legend, the reader is referred to the web version of the article).

significant effect on both HDS and HYD properties. The DBT HDS and naphthalene HYD rate constants increased from 1.8×10^{-5} mol h^{-1} g^{-1} (W_{12}/Al) to 6.2×10^{-5} mol h^{-1} g^{-1} and from 12.0 $\times 10^{-5}$ (W_{12}/Al) to 31.1 $\times 10^{-5}$ mol h^{-1} g^{-1} respectively for $Mo_1 + W_{11}/Al_2O_3$ catalyst and reached 8.0×10^{-5} and 38.5×10^{-5} mol h^{-1} g^{-1} with further tungsten replacement by molybdenum in $Mo_3 + W_9/Al_2O_3$. The catalytic activity of the reference catalysts is not a linear combination of those of the monometallic Mo_{12}/Al_2O_3 and W_{12}/Al_2O_3 solids. These results are opposed to those reported by Thomazeau et al. [2] who prepared mixed MoW/Al$_2$O$_3$ catalysts from solutions of separate precursors, ammonium heptamolybdate $(NH_4)_6Mo_7O_{24}$ and ammonium metatungstate $(NH_4)_6H_2W_{12}O_{40}$. Moreover, the introduction of Mo in our mixed Mo_xW_{12-x}/Al_2O_3 catalysts had a large beneficial effect leading to better catalytic activities both in HDS and HYD than its counterpart $Mo_1 + W_{11}/Al_2O_3$. The improved catalytic performances are still higher when comparing catalytic activities of Mo_3W_9/Al_2O_3 catalyst to that of $Mo_3 + W_9/Al_2O_3$. In this case, the Mo_3W_9/Al_2O_3 sample demonstrated the highest activity in HYD of naphthalene as well as a high HDS activity very close to that of Mo_{12}/Al_2O_3. These observations allowed us to conclude that the origin of the catalytic improvement is not only due to the simultaneous presence of Mo together with W as in reference $Mo + W/Al_2O_3$ catalysts but arises from the close interaction of both metals in the mixed HPA precursor supposed to form mixed

$Mo_xW_{-x}S_2$ active phase. The HAADF analysis evidenced the formation of mixed MoWS$_2$ slabs with WS$_2$ on the edges, with a more intimate mixture of Mo and W atoms in the slabs of the Mo_3W_9/Al_2O_3 sample compared to $Mo_3 + W_9/Al_2O_3$. It seems then that the use of the mixed HPA as precursor leads to a beneficial synergetic effect between the two metals.

Different dispersion of sulfided Mo(W)S$_2$ species witnesses in favor of dissimilar mechanism of catalysts sulfidation. Indeed, both $Mo_3 + W_9/Al_2O_3$ and $Mo_1 + W_{11}/Al_2O_3$ catalysts had the longest length slabs equal to 5.3 and 5.1 nm, respectively. Both Mo_3W_9/Al_2O_3 and Mo_1W_{11}/Al_2O_3 samples prepared from mixed $SiMo_nW_{12-n}$, by contrast, had the lowest particle size. These differences are accompanied by randomly Mo-W distribution into small slabs of Mo_3W_9/Al_2O_3 catalyst, compared to large Mo islands in the middle of W atoms and monometallic slabs in $Mo_3 + W_9/Al_2O_3$ as seen in HAADF images. The smaller size of particles in the catalysts prepared from mixed $SiMo_nW_{12-n}$ can be explained by simultaneous sulfidation of both Mo and W metals. In contrast, longer length in the catalysts prepared from the mixture of two HPA can be induced by sequential sulfidation of the metals when the growth of WS$_2$ particles proceeds on already formed large MoS$_2$ clusters.

Cyclic sulfur compounds react through two pathways: DDS and HYD. The ratio of DDS to HYD depends on the reactant molecules, the catalyst properties and the reaction conditions. The reaction pathways

Table 4
Metal fractions measured by XPS for molybdenum and tungsten species present at the surface of sulfided Mo_nW_{12-n}/Al_2O_3 catalysts.

Catalyst	Mo fraction (rel.%)			W fraction (rel.%)			Number of edge sites (10^{20} at g^{-1})		
	MoS_2	MoS_xO_y	Mo^{6+}	WS_2	WS_xOy	W^{6+}	Mo_{edge}^{IV}	W_{edge}^{IV}	$\Sigma\ Mo_{edge}^{IV} + W_{edge}^{IV}$
Mo_{12}/Al_2O_3	73	14	13	–	–	–	0.87	–	0.87
W_{12}/Al_2O_3	–	–	–	56	7	37	–	0.65	0.65
Mo_1W_{11}/Al_2O_3	100	–	–	73	3	24	0.12	0.78	0.90
Mo_3W_9/Al_2O_3	100	–	–	80	2	18	0.34	0.73	1.07
$Mo_1 + W_{11}/Al_2O_3$	100	–	–	74	2	24	0.13	0.66	0.79
$Mo_3 + W_9/Al_2O_3$	100	–	–	70	2	28	0.32	0.39	0.71

Table 5
Catalytic properties of prepared Mo_nW_{12-n}/Al_2O_3 catalysts in HDT of a mixture of DBT and naphthalene.

Catalyst	Conversion (%)		Selectivity ratio $S_{HYD/DDS}$	Rate constants ($\times 10^5$ mol h^{-1} g^{-1})		TOF values ($\times 10^4$ s^{-1})	
	DBT HDS	Naphthalene HYD		k_{HDS}	k_{HYD}	TOF_{HDS}	TOF_{HYD}
Mo_{12}/Al_2O_3	30.5	24.0	0.7	22.4	83.2	3.6	13.9
W_{12}/Al_2O_3	2.9	3.9	0.4	1.8	12.0	0.5	3.0
Mo_1W_{11}/Al_2O_3	15.7	17.2	1.4	10.5 (3.5*)	57.0 (17.9*)	1.8 (0.7*)	9.6 (3.9*)
Mo_3W_9/Al_2O_3	29.0	31.4	2.0	21.1 (6.9*)	114.0 (29.8*)	2.8 (1.2*)	14.8 (5.8*)
$Mo_1 + W_{11}/Al_2O_3$	9.6	9.8	0.6	6.2 (3.5*)	31.1 (17.9*)	1.3 (0.7*)	6.3 (3.9*)
$Mo_3 + W_9/Al_2O_3$	12.2	11.9	0.6	8.0 (6.9*)	38.5 (29.8*)	1.8 (1.2*)	8.5(5.8*)

*The additive quantities, which were calculated using the values for monometallic Mo_{12}/Al_2O_3 and W_{12}/Al_2O_3.

for DBT are shown in Scheme 1.

The selectivity ratios $S_{HYD/DDS}$ reported in Table 5 are of the same order of magnitude for Mo_{12}/Al_2O_3, W_{12}/Al_2O_3 and the reference catalysts with values between 0.4 and 0.7. Naphthalene was proposed to inhibit both direct desulfurization and prehydrogenation pathways to the same extent, as reported previously by several authors [19,20]. In mixed HPA based catalysts the selectivity ratio is largely higher than those obtained on monometallic and reference samples. Mo_3W_9/Al_2O_3 catalyst exhibits the highest $S_{HYD/DDS}$ value (2.05) among the prepared samples. This high value is typical of bulk sulfides having significant HYD activity. This observation supports the formation of a different active phase such as mixed $Mo_xW_{1-x}S_2$ possessing different hydrogenation properties. Such properties are required for the treatment of heavy fuels [21–23].

The introduction of one or three Mo atoms into the structure of the initial oxide precursor leads to an increase of the total number of edge sites more than 1.4 times compared to W_{12}/Al_2O_3 sample (Table 4). Moreover, the number of edge sites in the catalysts prepared from mixed HPAs was higher than that of their corresponding references obtained via the mixture of two monometallic HPA. In order to take into account these discrepancies and to correctly compare the catalytic results, TOF values normalized on the edge sites of perfect hexagons were calculated for all catalysts. The highest TOF values for the HDS and HYD reactions were achieved for the catalysts prepared from mixed $SiMo_nW_{12-n}$ precursors (Table 5). Using mixed molecular precursors where one or three W atoms were substituted to molybdenum one leads to an increase of the TOF number in the HDS of DBT and HYD of naphthalene at 3.6 (5.6) and 3.2 (4.9) times respectively, compared to W_{12}/Al_2O_3 sample. Both Mo + W reference catalysts had active sites with lower TOF values than their counterparts prepared using mixed $SiMo_nW_{12-n}$. Moreover, it should be mentioned that Mo_3W_9/Al_2O_3 catalyst indicated the close TOF values to the magnitude for the Mo_{12}/Al_2O_3 catalyst. In addition, the TOF values for bimetallic catalysts were calculated by additive way (Table 5). All bimetallic samples had active sites with higher TOF values than the predicted ones. However, the experimental values of the catalysts synthesized from mixed HPAs were higher more than 1.5 times than those obtained on their corresponding Mo + W references. Considering that the particle size and stacking number of the active phase was not precisely similar in the prepared catalysts series the high synergistic effect from the use of mixed HPAs might be a result of the formation of more dispersed $Mo(W)S_2$ particles exhibiting increased activity due to the particle size effect [15,24]. Fig. 5 shows the dependence of the TOF number in DBT HDS normalized on the edge sites of $Mo(W)S_2$ slabs over Mo_nW_{12-n}/Al_2O_3 catalysts on the average length and average stacking of the $Mo(W)S_2$ phase species. Even the highest activity corresponds to Mo_{12}/Al_2O_3 catalyst having low average length and high stacking number, it can be seen that prepared samples have different TOF numbers with similar morphological characteristics of $Mo(W)S_2$ slabs, e.g. comparing Mo_{12}/Al_2O_3 and Mo_3W_9/Al_2O_3 catalysts or $Mo_1 + W_{11}/Al_2O_3$ and $Mo_3 + W_9/Al_2O_3$. Therefore, the synergy in Mo_nW_{12-n}/Al_2O_3 catalysts is rather associated to the formation of a mixed $Mo_xW_{1-x}S_2$ active phase

with random Mo repartition in WS_2 slabs due to the proximity of Mo and W atoms in the HPA structure. It should be noted that on $Mo_3 + W_9/Al_2O_3$ catalysts Mo islands appeared larger and located in the core of the WS_2 slabs. Activity of this catalysts was much lower than Mo_3W_9/Al_2O_3 one with more homogeneous Mo-W distributions. Thus, our results clearly indicated that HDS and HYD activity of bimetallic MoW catalysts supported on Al_2O_3 correlated with the amount of $MoWS_2$ mixed sites.

5. Conclusions

The influence of the nature of mixed MoW oxide precursor on the catalytic activity of MoW catalysts supported on alumina has been investigated in the present study. The use of mixed $SiMo_nW_{12-n}$ for the preparation of bimetallic catalysts leads to a significant change in the composition of the sulfide particles of the active phase while maintaining similar dispersion compared to the monometallic analogues based on $SiMo_{12}$ and SiW_{12}. The tungsten sulfidation degree on the catalysts prepared with mixed HPA was higher by more than 24% compared to W_{12}/Al_2O_3. Moreover, HAADF images showed the formation of mixed $Mo_xW_yS_2$ slabs with Mo atoms distributed inside the WS_2 slabs.

$SiMo_nW_{12-n}$ based catalysts were more active in DBT HDS and naphthalene HYD reactions than their Mo + W references with the same metal surface density prepared from two separate monometallic HPA. The TOF values on Mo_3W_9/Al_2O_3 were similar to that of the Mo^{IV} sites on Mo_{12}/Al_2O_3 and higher by ~1.6 times compared to $Mo_3 + W_9/Al_2O_3$ sample. It has been found that the synergy in Mo_nW_{12-n}/Al_2O_3 catalysts is rather associated to the formation of a mixed $Mo_xW_{1-x}S_2$ active phase with random Mo repartition in WS_2 slabs due to the proximity of Mo and W atoms in the HPA structure. The selectivity ratio $S_{HYD/DDS}$ achieved on mixed $SiMo_nW_{12-n}$ based catalysts were at least twice higher than the values on all other samples, evidencing that homogeneously distributed mixed $MoWS_2$ active sites obtained from mixed HPA precursors as demonstrated by HAADF characterization, have enhanced HYD activity. Investigation of trimetallic $NiMo_nW_{12-n}/Al_2O_3$ catalysts prepared using mixed $SiMo_nW_{12-n}$ is under progress. Results will be published soon.
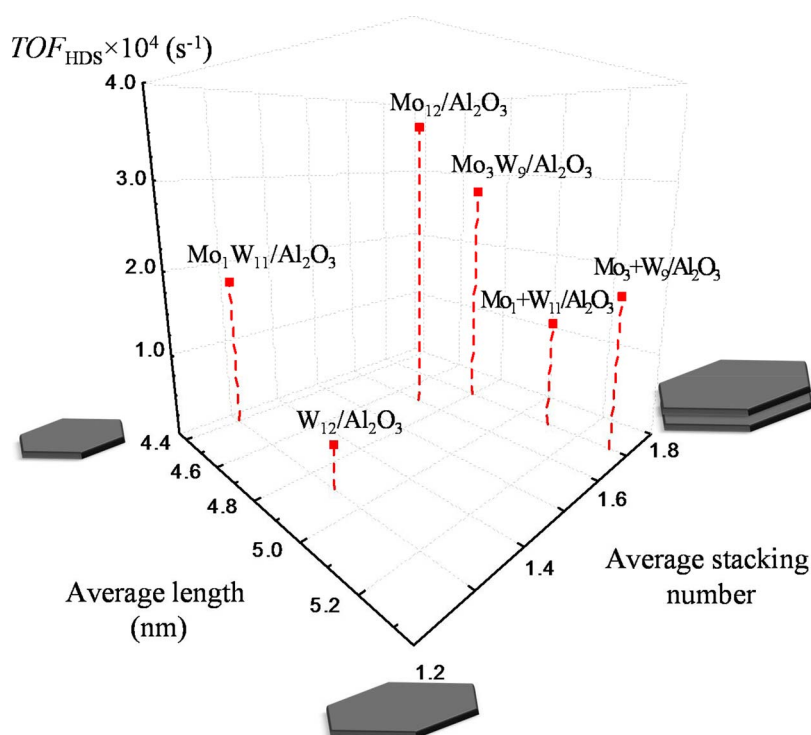
Fig. 5. 3D dependence of the TOF number in DBT HDS over Mo_nW_{12-n}/Al_2O_3 catalysts on the average length and average stacking number of the $Mo(W)S_2$ phase species.

in Russia for the Vernadsky fellowship and Haldor Topsøe Company for the grant to perform her PhD thesis.

References

[1] S. Eijsbouts, F. Plantenga, B. Leliveld, Y. Inoue, K. Fujita, STARS and NEBULA–new generations of hydroprocessing catalysts for the production of ultra low sulfur diesel, Prepr. Pap.-Am. Chem. Soc. Div. Fuel Chem. 48 (2) (2003) 494–495.

[2] C. Thomazeau, C. Geantet, M. Lacroix, M. Danot, V. Harle, P. Raybaud, Predictive approach for the design of improved HDT catalysts: γ-alumina supported (Ni, Co) promoted $Mo_{1-x}W_xS_2$ active phases, Appl. Catal. A 322 (2007) 92–97.

[3] A. Olivas, D.H. Galván, G. Alonso, S. Fuentes, Trimetallic NiMoW unsupported catalysts for HDS, Appl. Catal. A 352 (2009) 10–16.

[4] L. van Haandel, M. Bremmer, P.J. Kooyman, J.A.R. van Veen, T. Weber, E.J.M. Hensen, Structure-activity correlations in hydrodesulfurization reactions over Ni-promoted $Mo_xW_{(1-x)}S_2/Al_2O_3$ catalysts, ACS Catal. 5 (2015) 7276–7287.

[5] C. Sanchez, J. Livage, J.P. Launay, M. Fournier, Y. Jeannin, Electron delocalization in mixed-valence molybdenum polyanions, J. Am. Chem. Soc. 104 (11) (1982) 3194–3202.

[6] S. Kasztelan, H. Toulhoat, J. Grimblot, J.P. Bonnelle, A geometrical model of the active phase of hydrotreating catalysts, Appl. Catal. 13 (1984) 127–159.

[7] P.A. Nikulshin, A.V. Mozhaev, K.I. Maslakov, A.A. Pimerzin, V.M. Kogan, Genesis of HDT catalysts prepared with the use of $Co_2Mo_{10}HPA$ and cobalt citrate: study of their gas and liquid phase sulfidation, Appl. Catal. B 158–159 (2014) 161–174.

[8] P.P. Minaev, P.A. Nikulshin, M.S. Kulikova, A.A. Pimerzin, V.M. Kogan, NiWS/Al_2O_3 hydrotreating catalysts prepared with 12-tungstophosphoric heteropolyacid and nickel citrate: effect of Ni/W ratio, Appl. Catal. A 505 (2015) 456–466.

[9] A.V. Mozhaev, P.A. Nikulshin, Al.A. Pimerzin, K.I. Maslakov, A.A. Pimerzin, Investigation of co-promotion effect in NiCoMoS/Al_2O_3catalystsbased on Co_2Mo_{10}-heteropolyacid and nickel citrate, Catal. Today 271 (2016) 80–90.

[10] R. López Cordero, F.J. Gil Llambias, A. López Agudo, Temperature-programmed reductio and zeta potential studies of the structure of MoO_3/Al_2O_3 and MoO_3/SiO_2 catalysts: effects of the impregnation pH and molybdenum loading, Appl. Catal. 74 (1991) 125–136.

[11] R. López Cordero, A. López Agudo, Effect of water extraction on the surface properties of Mo/Al_2O_3 and $NiMo/Al_2O_3$ hydrotreating catalysts, Appl. Catal. A 202 (2000) 23–35.

[12] C.-H. Kim, W.L. Yoon, I.C. Lee, S.I. Woo, The effect of Ni loading and the sulfidation temperature on the structure and catalytic activity of NiW hydrodesulfurization catalysts, Appl. Catal. A 144 (1996) 159–175.

[13] A. Carlsson, M. Brorson, H. Topsøe, Supported metal sulfide nanoclusters studied by HAADF-STEM, J. Microscopy 223 (2006) 179–181.

[14] L.P. Hansen, Q.M. Ramasse, C. Kisielowski, M. Brorson, E. Johnson, H. Topsøe, S. Helvag, Atomic-scale edge structures on industrial-style MoS_2 nanocatalysts, Angew. Chem. Int. Ed. 50 (2011) 10153–10156.

[15] P. Raybaud, H. Toulhoat, Catalysis by Transition Metal Sulfides From Molecular Theory to Industrial Applications, Technip Edition, Paris, 2013 p. 832.

[16] P. Hartel, H. Rose, C. Dignes, Conditions and reasons for incoherent imaging in STEM, Ultramicroscopy 63 (1996) 93–114.

[17] A.J. van der Vlies, R. Prins, T. Weber, Chemical principles of the sulfidation of tungsten oxides, J. Phys. Chem. B 106 (2002) 9277–9285.

[18] M.J. Vissenberg, L.J.M. Joosten, M.M.E.H. Heffels, A.J. van Welsenes, V.H.J. de Beer, R.A. van Santen, J.A.R. van Veen, Tungstate versus molybdate adsorption on oxidic surfaces: a chemical approach, J. Phys. Chem. B 104 (2000) 8456–8461.

[19] H. Farag, I. Mochida, K. Sakanishi, Fundamental comparison studies on hydro-desulfurization of dibenzothiophenes over CoMo-based carbon and alumina catalysts, Appl. Catal. A 194–195 (2000) 147–157.

[20] M. Egorova, R. Prins, Competitive hydrodesulfurization of 4,6-dimethyldi-benzothiophene, hydrodenitrogenation of 2-methylpyridine, and hydrogenation of naphthalene over sulfided NiMo/γ-Al_2O_3, J. Catal. 224 (2004) 278–287.

[21] A. Varakin, P. Nikulshin, A. Pimerzin, V. Salnikov, A. Pimerzin, Hydrogen spillover effect in the presence of CoS_x/Al_2O_3 and bulk MoS_2 in hydrogenation, hy-drodenitrogenation and hydrodeoxygenation, Russ. J. Appl. Chem. 86 (2013) 718–726.

[22] T.C. Ho, J.M. McConnachie, Ultra-deep hydrodesulfurization on MoS_2 and $Co_{0.1}MoS_2$: intrinsic vs. environmental factors, J. Catal. 277 (2011) 117–122.

[23] S.L. Amaya, G. Alonso-Núnez, T.A. Zepeda, S. Fuentes, A. Echavarría, Effect of the divalent metal and the activation temperature of NiMoW and CoMoW on the di-benzothiophene hydrodesulfurization reaction, Appl. Catal. B 148–149 (2014) 221–230.

[24] P.A. Nikulshin, V.A. Salnikov, A.V. Mozhaev, P.P. Minaev, V.M. Kogan, A.A. Pimerzin, Relationship between active phase morphology and catalytic prop-erties of the carbon–alumina-supported Co(Ni)Mo catalysts in HDS and HYD reac-tions, J. Catal. 309 (2014) 386–396.